Robust topological surface states in Sb_2Te_3 layers as seen from the weak antilocalization effect

Y. Takagaki, A. Giussani, K. Perumal, R. Calarco, and K.-J. Friedland
Paul-Drude-Institut für Festkörperelektronik, Hausvogteiplatz 5-7, 10117 Berlin, Germany
(Received 27 July 2012; published 27 September 2012)

Weak antilocalization and electron-electron interaction effects are investigated in Sb_2Te_3 layers. We accomplish smooth top and bottom surfaces for the layer using molecular-beam epitaxy, as revealed by the Kiessig oscillations in the x-ray reflectivity. The two helical surface states of the layer are found to contribute identically to the weak antilocalization effect. They are left intact in spite of low mobility and high concentration of unintentionally doped holes. The magnitude of the electron-electron interaction effect is consistent with the indication that both of the surface states survive in the layer. The robustness of the surface states demonstrates superiority of Sb_2Te_3 over Bi_2Se_3 and Bi_2Te_3. We also show that the phase-change property of Sb_2Te_3 provides controllability to switch the existence of the surface states.

DOI: 10.1103/PhysRevB.86.125137 PACS number(s): 73.20.Fz, 73.50.Jt, 73.61.Le

I. INTRODUCTION

Topological insulators (TIs) are a new class of material for which gapless conductive surface states exist including the bulk band-gap region.[1] The surface states are helical. The spin-momentum locking is attractive for spintronic applications as electrical manipulation of the spin without relying on external magnetic fields or ferromagnetic materials becomes feasible. The helicity also protects the surface states from backscattering caused by nonmagnetic impurities.

The π Berry phase associated with the helical surface states gives rise to a quantum correction to the conductivity at low temperatures.[2,3] Its temperature and magnetic-field dependencies are identical in form to those of the weak antilocalization (WAL) effect in a two-dimensional (2D) system having strong spin-orbit interaction.[4] Specifically, the magnitude depends on temperature T as

$$\delta\sigma_{\mathrm{L}}(T) = -\alpha \frac{e^2}{\pi h} \ln\left(\frac{\tau_\phi}{\tau}\right) = \alpha p \frac{e^2}{\pi h} \ln\left(\frac{T}{T_{\mathrm{L}}}\right), \quad (1)$$

where τ is the elastic scattering time. We have assumed the phase coherence time τ_ϕ to vary with T as $\propto T^{-p}$ with T_{L} being a characteristic temperature. The WAL effect is suppressed when the time-reversal symmetry is broken by a magnetic field B, resulting in a magnetoconductivity $\Delta\sigma_{\mathrm{L}}(B) = \delta\sigma_{\mathrm{L}}(B) - \delta\sigma_{\mathrm{L}}(B=0)$ described as

$$\Delta\sigma_{\mathrm{L}}(B) = \alpha \frac{e^2}{\pi h}\left[\psi\left(\frac{1}{2} + \frac{\hbar}{4eBL_\phi^2}\right) - \ln\left(\frac{\hbar}{4eBL_\phi^2}\right)\right], \quad (2)$$

where $\psi(x)$ is the digamma function and $L_\phi = (D\tau_\phi)^{1/2}$ is the phase coherence length with D being the diffusion constant.

The coefficient α was theoretically predicted to be $-\frac{1}{2}$ for a single helical surface state.[2,3] This implies that α should be -1 for a TI layer as one surface state exists at each side of the layer. The WAL effect has indeed been observed experimentally in thin layers of three-dimensional (3D) TIs Bi_2Se_3 and Bi_2Te_3. (Thin layers were required there to reduce the fraction of the bulk conduction as the materials were unintentionally doped.) However, the values of α reported so far are typically around $-1/2$; see Table I. This led to a speculation that one surface of the experimental layers was strongly disordered, and so the helical state at the side was destroyed.[5] Alternatively, the system may have acted as a single 2D state as the two surface states were almost completely mixed through the bulk states by frequent disorder scattering.[6]

While density-functional calculations have predicted Bi_2Se_3, Bi_2Te_3, and Sb_2Te_3 to be 3D TIs,[7,8] Sb_2Te_3 has received little attention so far. This may have resulted from the fact that the Fermi level in Sb_2Te_3 is located in the valence band. The material is regrettably unsuitable for examining the Dirac point using the angle-resolved photoemission spectroscopy,[9] which has proved to be a powerful tool by visualizing the spin texture associated with the Dirac cones in Bi_2Se_3 and Bi_2Te_3.[1] Nonetheless, a recent scanning-tunneling-microscopy investigation has revealed that the Dirac point in Sb_2Te_3 is located in the bulk band gap with large energy separations from the band edges.[10] This is similar to Bi_2Se_3 and more favorable than Bi_2Te_3, in which the Dirac point is situated in the vicinity of the valence-band edge.[9] Although Sb_2Te_3 has been investigated already for decades because of the thermoelectric[12] and phase-change properties,[13] there is no report on the transport properties from the viewpoint of TIs.

In this paper, we investigate the low-temperature transport properties in thin layers of Sb_2Te_3. The value of α obtained from the WAL effect in our Sb_2Te_3 layer is -1, i.e., both of the helical surface states appear to be preserved. As we show below, this is rather surprising as the mobility and concentration of free carriers in the layer are about one order of magnitude smaller and larger, respectively, than those typically realized in Bi_2Se_3 layers. We analyze the temperature dependence of the conductivity stemming from the electron-electron interaction (EEI) effect to support the finding that both of the surface states are relevantly involved. In addition, we show that the phase-change property of Sb_2Te_3 can be utilized to manipulate the surface states.

II. LAYER PREPARATION

We employed molecular-beam epitaxy (MBE) and hot-wall epitaxy (HWE) to prepare Sb_2Te_3 layers. The layer on which we focus most of our attention was grown by MBE due to the outstanding controllability of the layer thickness and the capability to monitor the growth *in situ* to achieve atomically flat surfaces.

 ©2012 American Physical Society

TABLE I. Values of α reported for weak antilocalization effect in TI layers. The conduction was n-, n-, and p-type in the Bi_2Se_3, Bi_2Te_3, and Sb_2Te_3 layers, respectively.

TI layer	Substrate	Reference	$-\alpha$
Bi_2Se_3	Al_2O_3	42	0.3
Bi_2Se_3	SiC(0001)	32	0.31
Bi_2Se_3	InP(111)A	43	0.31
Pb-doped Bi_2Se_3	SiC(0001)	32	0.35
Bi_2Se_3	Al_2O_3(0001)	44	0.40
Bi_2Se_3	Al_2O_3	45	0.3 ∼ 0.6
Bi_2Se_3	$SrTiO_3$(111)	46	1/2
Bi_2Se_3	Si(111)	47	∼1/2
Cu-doped Bi_2Se_3	Si(001)	33	0.55
Bi_2Se_3	$SrTiO_3$(111)	23	1/2 ∼ 1
Bi_2Se_3		24	1/2 ∼ 1
Bi_2Se_3	Si(111)	25	0.7 ∼ 1
Bi_2Se_3		48	1.3
Bi_2Te_3	GaAs(111)	5	0.39
Sb_2Te_3	Si(111)	This work	1

The substrates used in the MBE growth were Si(111) wafers (resistivity $>5 \times 10^5$ Ωm) protected by a 100-nm-thick SiO_2 cap layer. Prior to loading into the MBE setup, the substrates were first cleaned in a Piranha-etch solution in order to remove organic contaminants. They were then dipped in 5%-diluted HF to strip the thermal oxide.[11] Moisture was outgassed in the load-lock of the MBE setup by means of an annealing at 350°C. The substrates were subsequently transferred into the growth chamber (base pressure $\sim 10^{-10}$ mbar) and heated up to 720°C at a rate of 0.1°C/s to prepare a (7×7)-reconstructed surface.[14] The Sb_2Te_3 layers were deposited using Sb and Te fluxes supplied by the dual-filament effusion cells to prevent material condensation at the orifices. The substrate temperature was 250°C and the Sb-to-Te flux ratio was ∼0.7. These conditions yielded a growth rate of 0.35 nm/min. The growth process was monitored in real time by means of the *in situ* reflection high-energy electron diffraction and quadrupole mass spectrometry.

For comparison, we also examine the transport properties in a Sb_2Te_3 film grown by HWE. The growth in HWE takes place under thermodynamical equilibrium conditions.[15] For HWE, the source and substrates were placed in an evacuated quartz tube having an inner diameter of 21 mm. (The pressure was $\sim 10^{-2}$ mbar.) The distance between the source (2 g Sb_2Te_3 pieces) and the Si(111) substrate was about 20 cm. We removed the native oxides of the substrate using a 5% HF solution immediately before the mounting. The growth was carried out by heating the source and substrate regions to about 500 and 300°C, respectively, using a horizontal three-zone furnace for 8.5 h.[16]

The MBE-grown layer was characterized *ex situ* by means of x-ray-diffraction and x-ray-reflectivity (XRR) specular ω-2θ scans,[17] as shown in Figs. 1(a) and 1(b), respectively. We plot the data as a function of $Q_z = (4\pi/\lambda)\sin\theta\cos(\omega - \theta)$.[18] The measurements were carried out in the double-axis configuration using the Cu $K\alpha_1$ radiation (wavelength $\lambda = 0.1540598$ nm) and a Ge(220) hybrid monochromator. For XRR, the signal is acquired using a parallel plate collimator.

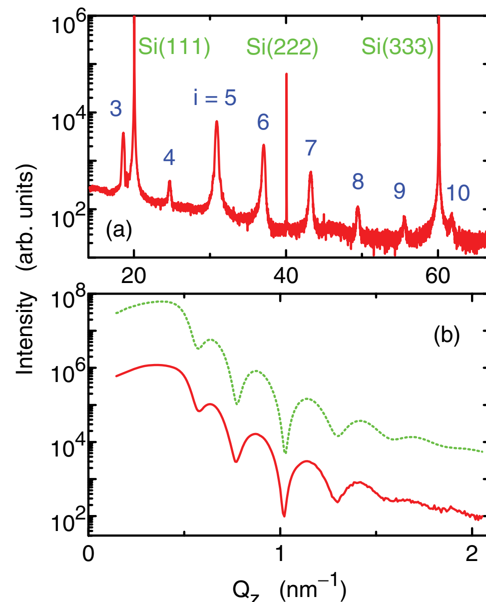

FIG. 1. (Color online) Specular ω-2θ scans of (a) x-ray diffraction and (b) x-ray reflectivity. The Sb_2Te_3 layer was grown on Si(111) by MBE. The data are shown as a function of $Q_z = (4\pi/\lambda)\sin\theta\cos(\omega - \theta)$, where $\lambda = 0.1540598$ nm is the wavelength of the x-ray. The $Sb_2Te_3(00.3i)$ peaks are identified in addition to the peaks associated with the substrate in (a). The dotted curve in (b) shows the fitting result. The curve is offset, for clarity.

In Fig. 1(a), one finds peaks associated with the $Sb_2Te_3(00.3i)$ Bragg reflections in addition to the reflections arising from the substrate. The Sb_2Te_3 layer is thus demonstrated to have grown in the rhombohedral phase with exclusively the C-plane orientation of hexagonal crystal. The out-of-plane lattice parameter of the layer is calculated to be 3.050 nm, which is about 0.16% larger than the bulk value.

The Kiessig oscillations in Fig. 1(b) demonstrate smoothness of the top and bottom surfaces of the layer. The dotted curve shows the result of fitting.[19] The layer thickness is estimated to be 21 nm with the roughnesses of the layer-substrate interface and the top surface of 0.2 and 1.5 nm, respectively. [We show the scanning electron micrograph of the surface in the inset of Fig. 2(a).] The physical density of the material obtained from the fitting (6.02 g/cm^3) was about 90% of the bulk value (6.691 g/cm^3). We point out that taking into account only one layer was sufficient to fit the curve. This means that the oxidation at the surface was small. In addition, there was no compositional gradient in the layer nor a significant interfacial layer adjacent to the substrate.

III. TRANSPORT PROPERTIES

The transport coefficients were measured using the lock-in technique. The magnetic field was applied normal to the surface. We used the van der Pauw method in order to avoid the contamination of the surface, which is inevitable if Hall bars are fabricated using the lithography and etching techniques. For this reason, Au leads were bonded directly to the layer without preparing contact pads. This turned out to be an easy task as Sb_2Te_3 is markedly soft.

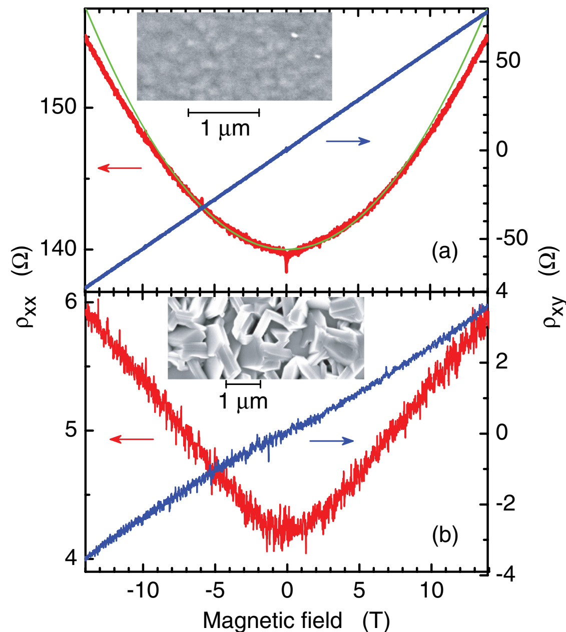

FIG. 2. (Color online) Dependencies of longitudinal resistivity ρ_{xx} and transverse resistivity ρ_{xy} on magnetic field at temperature of 0.32 K. The samples are (a) 21-nm-thick Sb_2Te_3 layer grown by MBE and (b) Sb_2Te_3 film grown by HWE. The thin curve in (a) demonstrates the parabolic dependence. The insets are scanning electron micrographs of the sample surfaces.

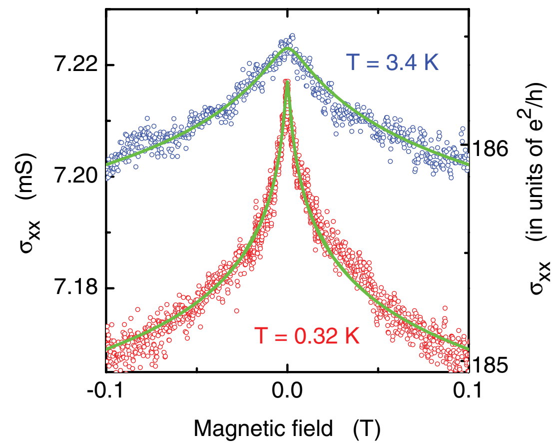

FIG. 3. (Color online) Dependence of longitudinal conductivity σ_{xx} on magnetic field in 21-nm-thick Sb_2Te_3 layer grown by MBE. The temperature was $T = 0.32$ and 3.4 K. The curves show fits using Eq. (2).

In Fig. 2(a), we show the magnetotransport properties in the 21-nm-thick MBE-grown layer at a temperature of 0.32 K. The Sb vacancies and Sb_{Te} antisite defects in the Sb_2Te_3 lattice generate free carriers.[20] Undoped Sb_2Te_3 layers thus exhibit p-type conduction. The longitudinal resistivity ρ_{xx} changes nearly parabolically with B, as manifested by the thin curve. The magnetic-field dependence of the transverse resistivity ρ_{xy} was almost completely linear for the whole range of measurements performed up to 14 T. The mobility and concentration of holes were derived to be 0.040 m^2/Vs and 5.3×10^{25} m^{-3}, respectively. Despite such a high hole concentration, one type of holes is suggested to overwhelm the classical magnetotransport phenomena in ρ_{xx} and ρ_{xy}. The mobility estimated from the parabolic magnetic-field dependence in ρ_{xx} is 0.025 m^2/Vs. The reasonable agreement of the mobilities estimated using the two methods affirms the dominance of one type of hole in the transport properties.

For comparison, we show in Fig. 2(b) the magnetotransport properties in the Sb_2Te_3 film grown by HWE. As shown in the inset of Fig. 2(b), the film consists of submicrometer-size disks. The disk geometry reflects the hexagonal crystal of Sb_2Te_3. The self-organized disk formation was prompted by the large lattice-mismatch strain between the $Sb_2Te_3(0001)$ and Si(111) planes.[16] While we are unable to estimate the hole concentration as the film thickness is undeterminable due to the porosity,[21] the nominal mobility is obtained to be 0.057 m^2/Vs. The mobility in the HWE-grown film is thus larger than that in the MBE-grown layer. This highlights the fact that the dominant scatterers are the charged vacancies that generated the holes rather than residual impurities. The deviation of the parabolic dependence in ρ_{xx} occurs in Fig. 2(b) at a weaker magnetic field in comparison to that in Fig. 2(a). Considering the mobility difference, the onset of the regime of Shubnikov-de Haas oscillations may be responsible for the deviation. However, the possibility of more than one type of carriers being involved in the transport processes cannot be ruled out in Fig. 2(b) as the magnetic-field dependence of ρ_{xx} is linear over a wide range and that of ρ_{xy} is somewhat nonlinear.

The sharp cusp in ρ_{xx} that one finds around zero magnetic field in Fig. 2(a) originates from the WAL effect.[21] In Fig. 3, we show the WAL effect with an expanded field scale together with its temperature dependence. Here, σ_{xx} is the longitudinal conductivity. The solid curves display the results of fitting using Eq. (2). Remarkably, the value of α was found to be -1. As $\alpha = -1$ is accomplished only when there exist two identical 2D conduction channels, the WAL effect is confirmed to be associated with the helical surface states at the two sides of the layer.

Apart from the fact that $\alpha \approx -1/2$ has been fairly consistently observed in Bi_2Se_3 and Bi_2Te_3 layers, the decoupling of both of the surface states from the bulk states is rather unexpected in the Sb_2Te_3 layer. The hole concentration in Sb_2Te_3 is typically on the order of 10^{25} m^{-3}.[22] The large hole concentration implies that the Fermi level in the valence band is located considerably away from the band edge. One may hence anticipate that the surface states would be strongly mixed with the bulk states, in particular, given the low hole mobility.

All the observations of $\alpha = -1$ in Bi_2Se_3 layers summarized in Table I were achieved when the electron density in the bulk was reduced by applying negative gate biases to the layers.[23–25] This may suggest that the appearance of the WAL effect as if being associated with a single surface state was a consequence of the coupling of the two surface states via the bulk states. As we find $\alpha = -1$ in the Sb_2Te_3 layer in spite of the unfavorable conditions in the mobility and concentration of the holes, it is worthy to point out that the exposure of the Bi_2Se_3 surface to the atmosphere has been revealed to give rise to the formation of a surface inversion layer.[26–28] The

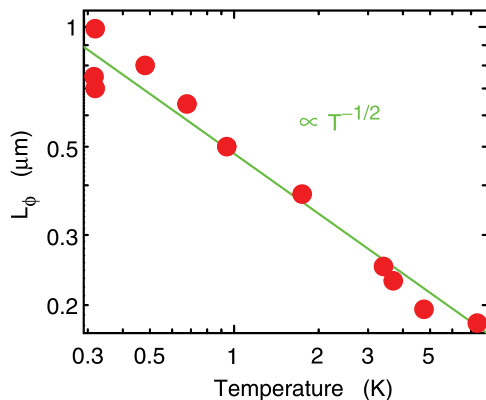

FIG. 4. (Color online) Temperature dependence of phase coherence length L_ϕ in 21-nm-thick Sb_2Te_3 layer grown by MBE. The solid line shows the prediction of the two-dimensional electron-electron Nyquist dephasing, which gives rise to the power-law dependence $\propto T^{-1/2}$. The theoretical value was multiplied by a factor of 0.65.

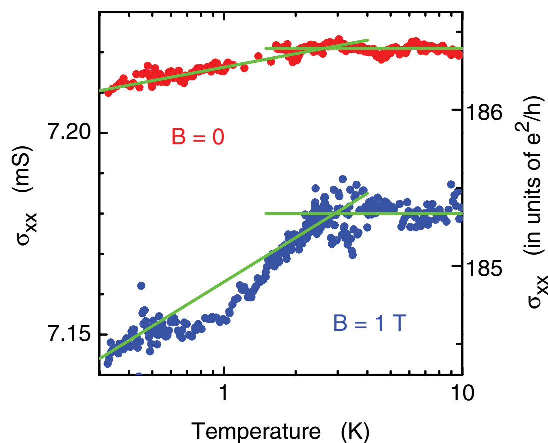

FIG. 5. (Color online) Temperature dependence of longitudinal conductivity σ_{xx} in 21-nm-thick Sb_2Te_3 layer grown by MBE. The magnetic field B applied normal to the surface is 0 and 1 T. The lines are guides for the eyes.

quasi-2D subbands in the inversion layers will likely enhance the coupling of the helical surface states with the bulk states.[29] Therefore, the readily accomplished $\alpha = -1$ may suggest that Sb_2Te_3 is less vulnerable against exposure to atmosphere. Alternatively, the realizations of $\alpha = -1$ in Sb_2Te_3 layers and in Bi_2Se_3 layers under negative gate biases may indicate that disorder is less effective for coupling the helical surface states with the valence-band states in comparison to with the conduction-band states.

We show the temperature dependence of L_ϕ in Fig. 4. The dependence of $L_\phi \propto T^{-1/2}$, which is indicated by the solid line, is in agreement with the expectation that the dephasing is governed by the 2D electron-electron scattering. The Nyquist dephasing rate due to the 2D electron-electron interaction is given by[30]

$$\tau_N^{-1} = k_B T \frac{e^2 \rho_s}{2\pi\hbar^2} \ln\left(\frac{\pi\hbar}{e^2\rho_s}\right), \qquad (3)$$

where ρ_s is the sheet resistivity. The solid line in Fig. 4 shows, in fact, the theoretical prediction multiplied by a factor of 0.65. We assumed the electronic state to be 3D in the calculation. (The theoretical value is about three times larger if the electronic state is assumed to be 2D.) We used the bulk hole effective mass $m^* = 0.78\, m_e$ in calculating D.[31] The effective mass of the upper and lower valence bands in Sb_2Te_3 is anisotropic and varies from $m^* = 0.034 m_e$ to $m^* = 1.24 m_e$.[31] This is likely to be one of the origins for the quantitative discrepancy. As the agreement is fairly good, although we used for ρ_s the value for the bulk states, the dephasing of the helical surface states is indicated to be dominated by the Coulomb collisions with the bulk states.

It is known that the Coulomb interactions in a disordered system yield another quantum correction to σ_{xx}. We now examine the interaction effect to find out if the presence of the two uncoupled surface states evidenced by the WAL effect is consistent with the temperature dependence generated by the EEI effect. As shown in Fig. 5, σ_{xx} decreases with lowering T. The temperature dependence is stronger when the WAL effect is quenched in the presence of a magnetic field. The conductivity correction due to the 2D EEI is given by[4]

$$\delta\sigma_I(T) = -\frac{e^2}{\pi h} n \left(1 - \frac{3}{4}F\right) \ln\left(\frac{T}{T_I}\right), \qquad (4)$$

where F is the screening factor and should lie between 0 and 1. We denoted the characteristic temperature for the interaction effect as T_I. We assume the number of 2D states to be $n = 2$ as $\alpha = -1$.

As plotted in Fig. 6, the amplitude f of the logarithmic temperature dependence $-[e^2/(\pi h)] f \ln(T/T_0)$ increases when a magnetic field is applied. It saturates as the WAL effect is quenched for $B > 0.1$ T. The magnetic-field dependence of the EEI effect is weak, and so the difference in f between the absence and presence of the magnetic field is attributed to the WAL effect. Using Eq. (1) with $p = 1$, we find $\alpha = -1.0 \sim -0.7$, which is reasonably close to the value of -1 obtained from the magnetoconductivity. From the saturation value of f in high magnetic fields, we obtain $F \sim 0.5$, which is also reasonable.[32]

The observation of $f > 1$ implies that the amplitude of the EEI effect becomes unaccountably large if the effect is

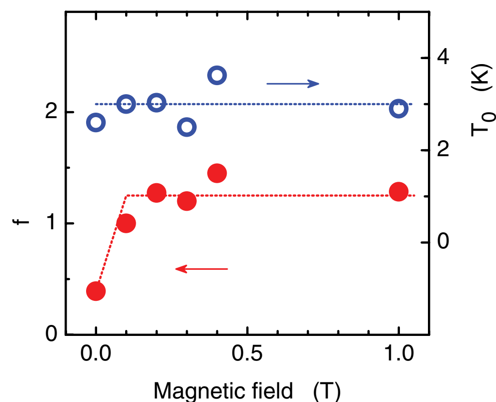

FIG. 6. (Color online) Dependence of parameters f and T_0 associated with logarithmic temperature dependence of conductivity $\sigma_{xx}(T) = -[e^2/(\pi h)] f \ln(T/T_0)$ on magnetic field. The lines are guides for the eyes.

attributed to a single 2D state, i.e., $n = 1$. This was the situation in our previous study of the WAL and EEI effects in Cu-doped Bi_2Se_3 layers.[33] The magnitude of the EEI effect was too large to be produced by one 2D state although the WAL effect indicated the presence of only one surface state. It may be, therefore, speculated that each of the surface states contributes to the EEI effect independently even when the two states are mixed in terms of the WAL effect.

We emphasize that the magnitudes of the quantum corrections can be satisfactorily explained by considering only the two surface states, as we described above. That is, we find no indication of the localization and interaction effects associated with the bulk states. The bulk contributions can be, in principle, two-dimensional[4,34] as the layer thickness is smaller than L_ϕ and the thermal diffusion length.[33] (We again emphasize that $\alpha = -1$ is achieved only if the contributions from two transport channels are identical. It is very unlikely that the contributions from the surface state and the bulk state become identical.) Lu and Shen[35] have shown theoretically that the bulk states may give rise to a weak localization (WL) effect despite the strong spin-orbit coupling. They argued that the universal experimental observation of $|\alpha| < 1$ that can be even $\alpha \sim -0.3$ is indication of the bulk contribution. Our observation of $\alpha = -1$ in the Sb_2Te_3 layer provides a possibility to test the applicability of the theory.

The bulk contribution to the WAL effect may become irrelevant if the bulk states are strongly localized by disorder. However, the transport properties plotted in Fig. 2(a) unambiguously indicate that the conduction in the bulk is in the metallic regime, i.e., the low mobility in the Sb_2Te_3 layer is still much larger than the mobility anticipated in the strongly localized regime. In Bi_2Se_3 layers, the dominant scattering in electrical conduction arises from the charged Se vacancies that have provided the free electrons. The electron mobility in Bi_2Se_3 layers was thus reported in some cases to be as low as the hole mobility in our Sb_2Te_3 layer. In addition, the counter doping to compensate the bulk carriers is know to dramatically lower the mobility. For instance, the mobility in the Cu-doped Bi_2Se_3 layer in Ref. 33 was only by about a factor of 2 larger than that in the Sb_2Te_3 layer. While the mobility in the previously investigated Bi_2Se_3 layers spread over a few orders of magnitude, there is no evidence so far that the mobility affects the value of α.

In evaluating the possible contributions of the bulk states, Sb_2Te_3 could be interesting as the spin-orbit coupling in Sb_2Te_3 is weaker than that in Bi_2Se_3 and Bi_2Te_3. In ordinary 2D systems, the WAL effect is a manifestation of strong spin-orbit coupling. If the spin-orbit coupling is moderately strong, the quantum correction behaves as a mixture of the WL and WAL effects, where the magnetoconductivity is *M*-shaped.[34] If the WAL effect in TI layers originates, at least in part, from the bulk spin-orbit coupling rather than from the π Berry phase associated with the surface states, the magnetoconductivity may develop a WL behavior when the spin-orbit coupling is only moderately strong. The double peaks in $\sigma_{xx}(B)$ were, however, not encountered throughout the measurements performed in the present study. (We ought to point out that, although the spin-orbit coupling in Sb is weaker than that in Bi, pure negative magnetoconductivity has been observed not only in Bi films[36] but also in Sb films.[37–40])

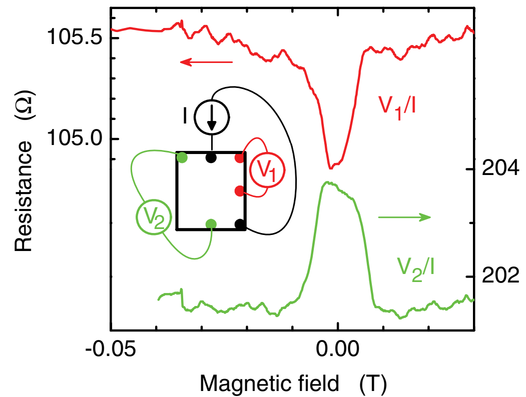

FIG. 7. (Color online) Weak localization and weak antilocalization effects in 21-nm-thick Sb_2Te_3 layer grown by MBE at a temperature of 0.32 K. Inhomogeneous phase changes were induced in the layer by applying large electrical pulses prior to the measurements. The sample is a rectangular-shaped piece (4.5 × 4 mm). The inset illustrates the measurement configurations of the leads for voltages V_i and current I.

Sb_2Te_3 is a phase-change material,[13] and so one can annihilate and re-create the surface states repeatedly by altering the crystalline order. We show a preliminary result in Fig. 7 to demonstrate such a switching. Here, strong electrical pulses were applied to the Sb_2Te_3 layer prior to the measurements in an attempt to induce amorphization. The resistances that were measured as illustrated in the inset exhibit WAL for one combination of the contacts but WL for the other. It is thus demonstrated that, while the crystalline order in the layer was disturbed highly inhomogeneously,[41] the surface states were annihilated in the disordered region. The WAL associated with the surface states was thereby turned into a WL plausibly associated with the bulk states.

The resistance change caused by the electrical pulses was considerably small (a few tenths of a percent). This is evident from the fact that, while the phase change can alter the resistance by orders of magnitude, the two resistances in Fig. 7 differ by about a factor of 2 that corresponds to the difference in the distance between the voltage contacts. Slight amorphization is thus suggested to be sufficient to annihilate the helical surface states. Nevertheless, the almost complete disappearance of the spin-orbit coupling indicated by the pure WL effect is hardly expected even if the Sb_2Te_3 layer has been fully amorphized. Further systematic investigations of the influence of the phase change are needed for understanding the behavior in Fig. 7. That the WL behavior can appear in the layer having strong spin-orbit coupling may be a confirmation of the theory by Lu and Shen.[35]

IV. CONCLUSIONS

In conclusion, we have investigated the WAL and EEI effects in Sb_2Te_3 layers. Both of the quantum effects have indicated that the two helical surface states in the layer have been robustly maintained. Sb_2Te_3 is thus found to be a superior 3D TI as compared to Bi_2Se_3 and Bi_2Te_3, although the low mobility and high concentration of the unintentionally doped holes make it seem unfavorable. We point out that the elastic

scattering time in Sb_2Te_3 is, in fact, roughly comparable to that in Bi_2Se_3 and Bi_2Te_3, which are n-type doped, as the hole effective mass is considerably larger than the electron effective mass. Moreover, the nominal mobility is governed by the scattering caused by the crystalline defects in the interior of the layer. It thus does not necessarily reflect the quality of the surface states. In this regard, the x-ray-reflectivity scan has exhibited the Kiessig oscillations, evidencing that the two surfaces of the layer grown by MBE are markedly flat. This may have been helpful in not causing scattering to the surface states. With respect to the high hole concentration, it is worthy to note that the classical magnetic-field dependencies in ρ_{xx} and ρ_{xy} of the layer at high fields have exhibited simple single-carrier behaviors. Another advantage of Sb_2Te_3 is the phase-change property. It provides a convenient method to annihilate and re-create the surface states as one desires. Our observations will, therefore, bring more attention to Sb_2Te_3 to explore its TI properties.

---

[1] X.-L. Qi and S.-C. Zhang, Rev. Mod. Phys. **83**, 1057 (2011).
[2] E. McCann, K. Kechedzhi, V. I. Fal'ko, H. Suzuura, T. Ando, and B. L. Altshuler, Phys. Rev. Lett. **97**, 146805 (2006).
[3] G. Tkachov and E. M. Hankiewicz, Phys. Rev. B **84**, 035444 (2011).
[4] P. A. Lee and T. V. Ramakrishnan, Rev. Mod. Phys. **57**, 287 (1985).
[5] H.-T. He, G. Wang, T. Zhang, I.-K. Sou, G. K. L. Wong, J.-N. Wang, H.-Z. Lu, S.-Q. Shen, and F.-C. Zhang, Phys. Rev. Lett. **106**, 166805 (2011).
[6] Y. Takagaki, Phys. Rev. B **85**, 155308 (2012).
[7] H. Zhang, C.-X. Liu, X.-L. Qi, X. Dai, Z. Fang, and S.-C. Zhang, Nat. Phys. **5**, 438 (2009).
[8] W. Zhang, R. Yu, H.-J. Zhang, X. Dai, and Z. Fang, New J. Phys. **12**, 065013 (2010).
[9] D. Hsieh, Y. Xia, D. Qian, L. Wray, F. Meier, J. H. Dil, J. Osterwalder, L. Patthey, A. V. Fedorov, H. Lin, A. Bansil, D. Grauer, Y. S. Hor, R. J. Cava, and M. Z. Hasan, Phys. Rev. Lett. **103**, 146401 (2009).
[10] Y. Jiang, Y. Wang, M. Chen, Z. Li, C. Song, K. He, L. Wang, X. Chen, X. Ma, and Q.-K. Xue, Phys. Rev. Lett. **108**, 016401 (2012).
[11] W. Kern, *Handbook of Semiconductor Wafer Cleaning Technology* (Noyes Publications, Park Ridge, 1993).
[12] P. A. K. Moorthy and G. K. Shivakumar, Cryst. Res. Technol. **21**, 783 (1986).
[13] S. Fujimori, S. Yagi, H. Yamazaki, and N. Funakoshi, J. Appl. Phys. **64**, 1000 (1988).
[14] V. De Renzi, R. Biagi, and U. del Pennino, Surf. Sci. **497**, 247 (2002).
[15] A. Lopez-Otero, Thin Solid Films **49**, 5 (1978).
[16] Y. Takagaki, B. Jenichen, U. Jahn, M. Ramsteiner, K.-J. Friedland, and J. Lähnemann, Semicond. Sci. Technol. **26**, 125009 (2011).
[17] M. Birkholz, *Thin Film Analysis by X-Ray Scattering* (Wiley, Weinheim, 2006).
[18] M. Sztucki, Ph.D. thesis, Ludwig-Maximilians-Universität München, 2004.
[19] The simulation was carried out using Rocking and Reflectivity Simulation Software (RCRefSimW) provided by P. Zaumseil [IHP, Frankfurt (Oder)].
[20] Y. Jiang, Y. Y. Sun, M. Chen, Y. Wang, Z. Li, C. Song, K. He, L. Wang, X. Chen, Q.-K. Xue, X. Ma, and S. B. Zhang, Phys. Rev. Lett. **108**, 066809 (2012).
[21] The resistivities in Fig. 2(b) are a few orders of magnitude smaller than those in Fig. 2(a). This indicates that the film in Fig. 2(b) is too thick for the WAL effect to be relevant.
[22] N. Peranio, M. Winkler, Z. Aabdin, J. König, H. Böttner, and O. Eibl, Phys. Status Solidi A **209**, 289 (2012).
[23] J. Chen, X. Y. He, K. H. Wu, Z. Q. Ji, L. Lu, J. R. Shi, J. H. Smet, and Y. Q. Li, Phys. Rev. B **83**, 241304 (2011).
[24] J. G. Checkelsky, Y. S. Hor, R. J. Cava, and N. P. Ong, Phys. Rev. Lett. **106**, 196801 (2011).
[25] H. Steinberg, J.-B. Laloe, V. Fatemi, J. S. Moodera, and P. Jarillo-Herrero, Phys. Rev. B **84**, 233101 (2011).
[26] P. D. C. King, R. C. Hatch, M. Bianchi, R. Ovsyannikov, C. Lupulescu, G. Landolt, B. Slomski, J. H. Dil, D. Guan, J. L. Mi, E. D. L. Rienks, J. Fink, A. Lindblad, S. Svensson, S. Bao, G. Balakrishnan, B. B. Iversen, J. Osterwalder, W. Eberhardt, F. Baumberger, and P. Hofmann, Phys. Rev. Lett. **107**, 096802 (2011).
[27] H. M. Benia, C. Lin, K. Kern, and C. R. Ast, Phys. Rev. Lett. **107**, 177602 (2011).
[28] Z.-H. Zhu, G. Levy, B. Ludbrook, C. N. Veenstra, J. A. Rosen, R. Comin, D. Wong, P. Dosanjh, A. Ubaldini, P. Syers, N. P. Butch, J. Paglione, I. S. Elfimov, and A. Damascelli, Phys. Rev. Lett. **107**, 186405 (2011).
[29] They will, at least, affect the depth profile of the helical surface states due to the orthogonality.
[30] B. L. Altshuler, A. G. Aronov, and D. E. Khmelnitsky, J. Phys. C **15**, 7367 (1982).
[31] O. Madelung, *Semiconductors: Data Handbook*, 3rd ed. (Springer, Berlin, 2004).
[32] J. Wang, A. M. DaSilva, C.-Z. Chang, K. He, J. K. Jain, N. Samarth, X.-C. Ma, Q.-K. Xue, and M. H. W. Chan, Phys. Rev. B **83**, 245438 (2011).
[33] Y. Takagaki, B. Jenichen, U. Jahn, M. Ramsteiner, and K.-J. Friedland, Phys. Rev. B **85**, 115314 (2012).
[34] G. Bergmann, Phys. Rep. **107**, 1 (1984).
[35] H.-Z. Lu and S.-Q. Shen, Phys. Rev. B **84**, 125138 (2011).
[36] D. E. Beutler and N. Giordano, Phys. Rev. B **38**, 8 (1988).
[37] A. V. Butenko, E. I. Bukhshtab, and Y. F. Komnik, Sov. J. Low Temp. Phys. **9**, 52 (1983).
[38] Y. Liu, S. Takaoka, and K. Murase, Solid State Commun. **67**, 783 (1988).
[39] J. Liu, T. L. Meisenheimer, and N. Giordano, Phys. Rev. B **40**, 7527 (1989).
[40] B. A. Hermann, P. Haier, I. Didschuns, N. Esser, W. Richter, and K. Lüders, Phys. Status Solidi B **205**, 241 (1998).
[41] The amorphization was triggered by excessive Joule heating caused by the electrical pulses. It is speculated for the case shown in Fig. 7 that the crystalline order was significantly distorted in the interior region, whereas the heating in the border regions was below the amorphization threshold.
[42] S. Matsuo, T. Koyama, K. Shimamura, T. Arakawa, Y. Nishihara, D. Chiba, K. Kobayashi, T. Ono, C.-Z. Chang, K. He, X.-C. Ma, and Q.-K. Xue, Phys. Rev. B **85**, 075440 (2012).

[43] Y. Onose, R. Yoshimi, A. Tsukazaki, H. Yuan, T. Hidaka, Y. Iwasa, M. Kawasaki, and Y. Tokura, Appl. Phys. Express **4**, 083001 (2011).

[44] M. Liu, J. Zhang, C.-Z. Chang, Z. Zhang, X. Feng, K. Li, K. He, L. L. Wang, X. Chen, X. Dai, Z. Fang, Q.-K. Xue, X. Ma, and Y. Wang, Phys. Rev. Lett. **108**, 036805 (2012).

[45] M. Liu, C.-Z. Chang, Z. Zhang, Y. Zhang, W. Ruan, K. He, L. L. Wang, X. Chen, J.-F. Jia, S.-C. Zhang, Q.-K. Xue, X. Ma, and Y. Wang, Phys. Rev. B **83**, 165440 (2011).

[46] J. Chen, H. J. Qin, F. Yang, J. Liu, T. Guan, F. M. Qu, G. H. Zhang, J. R. Shi, X. C. Xie, C. L. Yang, K. H. Wu, Y. Q. Li, and L. Lu, Phys. Rev. Lett. **105**, 176602 (2010).

[47] Y. S. Kim, M. Brahlek, N. Bansal, E. Edrey, G. A. Kapilevich, K. Iida, M. Tanimura, Y. Horibe, S.-W. Cheong, and S. Oh, Phys. Rev. B **84**, 073109 (2011).

[48] D. Zhang, J. Wang, A. M. DaSilva, J. S. Lee, H. R. Gutierrez, M. H. W. Chan, J. Jain, and N. Samarth, Phys. Rev. B **84**, 165120 (2011).